

# Solving the Graph Isomorphism Problem with a Quantum Annealer

Itay Hen\* and A. P. Young

*Department of Physics, University of California, Santa Cruz, California 95064, USA*

We propose a novel method for a quantum annealer – an analog quantum computer based on the principles of quantum adiabatic evolution – to solve the Graph Isomorphism problem in which one has to determine whether two graphs are isomorphic (i.e., can be transformed into each other simply by a relabeling of the vertices). We demonstrate the capabilities of the method by analyzing several types of graph families, focusing on graphs with particularly high symmetry called strongly regular graphs (SRG's). We also show that our method is applicable to currently available quantum computers such as “D-Wave One” and suggest a way to test our hypothesis with existing resources.

## I. INTRODUCTION

Theoretical research on quantum computing is motivated by the exciting possibility that quantum computers may be able to perform certain tasks faster than classical computers. In recent years first steps have been taken towards the goal of experimentally realizing these computational advantages. However, to date the largest experimental implementations of scientifically meaningful quantum algorithms have used just a handful of qubits [1, 2], the reason being the tremendous technological challenges (the most crucial of which is overcoming quantum decoherence) that need to be defeated before a successful implementation of any solid-state quantum computer. The magnitude of these difficulties is also reflected by the plethora of rivaling candidates for stable scalable quantum computers that are now being considered. Among these are superconducting qubits [3], ion traps [4], optical lattices [5], quantum dots [6], nuclear magnetic resonance on molecules [1] and many others, to mention a few diverse examples. Another indication of the uncertainty in the direction towards which the quantum computers industry is headed can be found by noting that many different potential architectures have been proposed. Among them are circuit-based computers [7], measurement-based computers [8, 9], topological quantum computers [10, 11], and quantum ‘annealers’ [12, 13].

Of the myriad of candidates for successful quantum computing device, a potentially promising substitute for the ‘standard’ circuit-based quantum computer is the quantum annealer [12, 13], which is now on the cusp [2] of being able to run small-scale computing procedures on actual quantum annealing hardware. Quantum annealing machines are analog quantum computational devices designed to solve discrete combinatorial optimization problems using properties of quantum adiabatic evolution. They are based on a general approach widely known as the Quantum Adiabatic Algorithm (QAA), which was proposed by Farhi *et al.* [14] about a decade ago as a method for solving a *broad range* of optimization problems using a quantum computer.

Recently, a quantum annealing machine, based on liquid crystal nuclear magnetic resonance has been reported to successfully factor the number 143 using four spin-qubits [15]. A few months later, “D-Wave One”, a 108-qubit machine based on superconducting qubits [16] experimentally demonstrated the ability to compute two-color Ramsey numbers [2, 17] making it the largest experimental implementation of a scientifically meaningful quantum algorithm. While at present noise and decoherence in quantum annealing devices can not be controlled or corrected easily (caveats that also hinder circuit-based quantum computers), fast improvements in superconducting qubits offer a near term potential for machines with significantly lower levels of decoherence.

This recent reported success of quantum annealers serves today both as a source for skepticism as to the true ‘quantumness’ of the inner workings of these machines but also as a tremendous incentive for finding problems and setups that could be solved, possibly very efficiently, on a quantum annealer. Extensive research is therefore underway to design such setups that could provide clear-cut examples that would demonstrate unequivocally the abilities of quantum computing devices in general and quantum annealers in particular.

In this paper, we provide ‘a proof of concept’ for utilizing quantum annealers to solve one such problem, namely the Graph Isomorphism (GI) problem. We propose a novel way to attack the GI problem using a quantum annealer, i.e., utilizing the properties of quantum adiabatic evolution (this will be explained in detail in the next section). We demonstrate that a quantum annealer may be used to distinguish non-isomorphic graphs, and show how this could be done. The main advantage of the method proposed here is that it can be tested and extensively studied using *currently available* quantum annealing machines such as D-Wave One, which enables adiabatic computations of Ising-type models augmented by transverse constant magnetic fields [2].

The paper is organized as follows. In Sec. II we describe the Graph Isomorphism (GI) problem in some detail. In Sec. III we describe and then discuss the proposed method for solving the GI problem using quantum adiabatic evolution. We next present the results of the study in Sec. IV and derive some conclusions in Sec. V.

---

\*Electronic address: itayhe@physics.ucsc.edu

## II. THE GRAPH ISOMORPHISM PROBLEM

The GI problem is stated as follows: Given two graphs, one must determine whether or not they are isomorphic to each other, i.e., whether or not they can be obtained by one another by a relabeling of the vertices.

In the realm of classical computing, many special cases of GI have been shown to be solvable in a time that scales as a polynomial of the number of vertices, however the best *general* algorithm to date runs in time  $\mathcal{O}(c^{N^{1/2} \log N})$  (here,  $c$  is a constant and  $N$  is the number of vertices in the graphs being compared) [18]. It is therefore an extremely intriguing question to see whether a quantum computer could be used to solve this problem, and the efficiency in which it will do so. An attractive feature of the GI problem is its resemblance to the problem of integer factoring which was the first and most famous example to date of a quantum algorithm can solve a problem exponentially faster than the best known classical algorithm [19]. Like factoring, it is felt that the GI problem is unlikely to be NP-complete, since otherwise many complexity classes believed to be distinct would collapse. Specifically, it has been shown that if graph isomorphism were NP-complete, the polynomial hierarchy collapses to level two [20]. Furthermore, both GI and factoring can be viewed as hidden subgroup problems: whereas in GI one is looking for a hidden subgroup of the permutation group, in factoring one is looking for a hidden subgroup of the Abelian group.

This GI problem has been attacked by numerous methods inspired by classical as well as quantum physical systems. Rudolph [21] mapped the GI problem onto a system of hard-core atoms, where one atom was used per vertex, and atoms  $i$  and  $j$  interacted if vertices  $i$  and  $j$  were connected by edges. It was demonstrated that for some pairs of non-isomorphic graphs, sharing cospectral adjacency matrices does not lead to cospectrality of the transition matrix between three-particle states produced by the embedded Hamiltonian. Gudkov and Nussinov [22] proposed a classical algorithm to distinguish non-isomorphic graphs by mapping them onto various physical problems. Shiau *et al.* proved that the simplest classical algorithm fails to distinguish some pairs of non-isomorphic graphs and also proved that continuous-time one-particle quantum random walks cannot distinguish some non-isomorphic graphs [23–25]. More recently, it has been found that classical random walks and quantum random walks can exhibit qualitatively different properties [26–28]. From a standpoint of algorithms research, these disparities lead to situations in which algorithms implemented by quantum random walkers can be proven to run faster than the fastest possible classical algorithm [29–38].

## III. QUANTUM ADIABATIC EVOLUTION AND THE GI PROBLEM

In what follows we introduce the framework within which a quantum annealer could be tested as a solver for the GI problem. The method is based on assigning to each graph  $G$  a unique Hamiltonian  $\hat{H}(G)$  :

$$\hat{H}(G) = (1 - s)\hat{H}_d + s\hat{H}_p(G). \quad (1)$$

The above Hamiltonian is a linear interpolation between a 'driver' Hamiltonian which we take to be the standard choice for QAA algorithms, namely  $\hat{H}_d = \frac{1}{2} \sum_i \sigma_i^x$ , i.e., a transverse-field Hamiltonian, and a 'problem' Hamiltonian  $\hat{H}_p(G)$  that is constructed according to the topology of the graph that is to be tested (the details of this Hamiltonian will be discussed shortly). While the driver Hamiltonian is diagonal in the  $\prod \sigma^x$  basis, the problem Hamiltonian will be diagonal in the  $\prod \sigma^z$  basis.

In order to distinguish non-isomorphic graphs, we follow the QAA prescription and take the following course of action, known as quantum adiabatic evolution. The system is first prepared in the easily prepared ground state of the driver Hamiltonian  $\hat{H}_d$ . The adiabatic parameter  $s$  is then varied smoothly and slowly from 0 to 1 so that the Hamiltonian of the system is continuously modified from  $\hat{H}_d$  to  $\hat{H}_p(G)$ . If this process is done slowly enough, the adiabatic theorem of Quantum Mechanics (see, e.g., Refs. [39] and [40]) ensures that the system will stay close to the ground state of the instantaneous Hamiltonian throughout the evolution.

The premise of the method we suggest here is that the state of the system along the adiabatic evolution, i.e., the instantaneous ground state of the Hamiltonian, Eq. (1), stores enough information to reflect the complex structure of the graph-dependent problem Hamiltonian  $\hat{H}_p(G)$ , and that carefully chosen measurements along the adiabatic path will provide enough information to differentiate non-isomorphic graphs.

As for the 'problem' Hamiltonian, we find that a simple yet plausible choice for  $\hat{H}_p(G)$  would be

$$\hat{H}_p(G) = \sum_{\langle ij \rangle \in G} \sigma_i^z \sigma_j^z, \quad (2)$$

i.e., an Ising antiferromagnet on the edges of the graph.

The above Hamiltonian is of course only one possibility. However, it has the advantages of (i) using Ising spins which are simple to study and to implement experimentally and (ii) antiferromagnetic interactions which, on highly-connected graphs, tend to have highly frustrated ground-states because closed paths (along the edges) of odd length would make the system a spin glass [41–44]. Note also, that the Hamiltonian Eq. (1) is symmetric with respect to flipping all spins.

Several other methods normally also consider various choices of physically-inspired Hamiltonians embedded in

the graph structure. However these studies normally only access small subspaces of the Hamiltonian, based on conserved quantities such as number of particles, and look within subspaces invariant with respect to the particle-number operator (see, e.g., Refs. [21, 23, 37, 38]). Here, since no such conserved quantity exists the instantaneous ground state of the Hamiltonian for the different  $s$  values presumably reflects the full complexity of the graph that is tested.

For each of the graphs  $G$  that have to be distinguished, one performs multiple runs along the adiabatic path, performing various measurements at different values of  $s$  until sufficient statistics is gathered. Since each measurement collapses the state of the system, non-commuting measurements or measurements corresponding to different  $s$  values, require separate runs of the procedure. Since errors of the various measured quantities are inversely proportional to square root of the number of measurements, this number will be determined from the needed resolution.

In order to make sure that isomorphic graphs are recognized as such, the measurements must be invariant under a relabeling of the vertices of the graph (or equivalently the spins in the system). The most straightforward such quantity is the Hamiltonian, rendering the energy  $E = \langle \hat{H}(G) \rangle$  a ‘good’ measurable quantity. Here,  $\langle \cdot \rangle$  indicates the expectation value with respect the state of the system, i.e., the instantaneous ground-state, at a particular value of  $s$ . For the same reason, the classical ‘diagonal’ energy of the graph  $E_G = \langle \hat{H}_p(G) \rangle$  and  $M_x = 2\langle \hat{H}_d \rangle$ , the  $x$ -magnetization, are also suitable observables.

There are in fact many other quantities that respect the topology of the graph and are invariant under any relabeling of the vertices, that one could indeed measure. Some may prove to have more distinguishing capabilities than others, depending on the manner in which they ‘tap’ into the complexity of the structure of the graph in question.

Interestingly, we find that ‘good’ properties to be measured are the spin-glass order parameter, which we shall denote as  $Q_2$ .

$$\langle Q_2 \rangle = \frac{1}{1 - 1/N} \left( \frac{1}{N^2} \sum_{i,j} \langle \sigma_i^z \sigma_j^z \rangle^2 - 1/N \right), \quad (3)$$

and generalizing the above expression, the quantities  $\langle Q_{2n} \rangle = \frac{1}{N^{2n}} \sum_{i_1, i_2, \dots, i_{2n}} \langle \sigma_{i_1}^z \sigma_{i_2}^z \dots \sigma_{i_{2n}}^z \rangle^2$ , where  $n = 2, 3, 4 \dots$  also serve as distinguishing operators. Analogously, other types of operators that might work would be of the form:  $\langle Q' \rangle = \frac{1}{N^2} \sum_{i,j} \langle \hat{H}_p(G) \sigma_i^z \sigma_j^z \rangle^2$ . Each such measurable quantity, if measured sufficiently accurately, for different values of the adiabatic parameter  $s$ , serves as an additional ‘dimension’ of differentiability of the non-isomorphic graphs. Moreover, gathering statistics of these quantities for different values of  $s$  accesses indirectly the entire spectrum of  $\hat{H}_p(G)$  (unlike the

situation in classical or quantum random walks where the walkers are restricted to only a small subspace of the Hamiltonian).

In Sec. IV we will demonstrate that non-isomorphic graphs are indeed distinguished by accurate measurements of carefully chosen observables along the adiabatic path. In fact, we shall see that in most cases studying the limit  $s \rightarrow 1$  suffices.

## IV. RESULTS

In what follows we demonstrate the capabilities of the quantum annealer using analytical and numerical analyses of the scheme devised in the previous section, and applied to several types of graph families that are known to be hard to distinguish. Since the annealing process requires that the temperature of the system be well below the excitation gap of the system, in the following analysis we shall work at zero temperature, i.e., study only the ground-state properties of the various Hamiltonians we construct in the process.

For the smaller graphs (of  $N \leq 25$  vertices), we obtain measurement results pertaining to the quantum adiabatic evolution by employing exact-diagonalization or conjugate-gradient based minimization techniques on the Hamiltonians for various values of the adiabatic parameter  $s$ . Both techniques are however highly restrictive in the size of a matrix one can study. The specific variation of conjugate-gradient method we developed for this study in order to obtain highly accurate results for all the observables we measure, is discussed in detail in Appendix A for the convenience of the reader.

For graphs of more than 25 vertices, quantum Monte-Carlo techniques would usually be the method of choice for the accurate measurements of the various quantities. However, these were found by us to be rather inefficient in the interesting regions where the value of the adiabatic parameter is close to 1. We have been able to study sizes *a little* larger than 25 (up to 29) by leading-order degenerate perturbation theory about the limit  $s = 1$ . This calculation involves finding the subspace of ground states of  $\hat{H}_p(G)$ , which requires one to first calculate the energies of the  $2^N$  ‘classical’ states followed by further manipulation on the subspace spanned by the ground-state eigenvectors. The main shortcoming of the method is that it only produces results in the  $s \rightarrow 1$  limit. Fortunately, we find that in most cases this is sufficient.

The measured quantities we focus on are the total energy, the spin-glass order parameter  $Q_2$  given in Eq. (3) and the  $x$ -magnetization  $M_x = 2\langle \hat{H}_d \rangle$ . We find that in most cases these two quantities are sufficient to distinguish all tested non-isomorphic graphs, though these measurements may be augmented by measuring other observables, as discussed in the previous section, to further differentiate non-isomorphic graphs.

### A. Strongly regular graphs

The main results of this paper focus on algorithms over strongly regular graphs (SRGs), a class of graphs, subsets of which are known to be difficult to distinguish [24]. An SRG is a graph in which (i) all vertices have the same degree, (ii) each pair of neighboring vertices has the same number of shared neighbors, and (iii) each pair of non-neighboring vertices has the same number of shared neighbors. This definition permits SRGs to be categorized into families by four integers  $(N, k, \lambda, \mu)$ , each of which might contain many non-isomorphic members. Here,  $N$  is the number of vertices in each graph,  $k$  is the degree of each vertex ( $k$ -regularity),  $\lambda$  is the number of common neighbors shared by each pair of adjacent vertices, and  $\mu$  is the number of common neighbors shared by each pair of non-adjacent vertices (more details on SRGs can be found in Appendix B). While there exist SRG families with only one non-isomorphic member [45], we concern ourselves with families that have more than one non-isomorphic graph. Complete and partial families of SRGs have been tabulated through combinatorial techniques [46, 47], which we use in what follows to perform numerical tests of our algorithms. It should be noted that, for every family of non-isomorphic SRGs, there exists a complementary family of the same size  $N$  and the same number of members, that is obtained by interchanging edges and non-edges.

The smallest family of non-isomorphic SRGs that have more than one member is that of the  $N = 16$  vertices with signature  $(16, 6, 2, 2)$ , which contains two members (we shall not address here the complementary families of graphs). The two graphs are immediately distinguished by looking for example at the spin-glass order parameter  $Q_2$  as a function of the adiabatic parameter  $s$  which reveals a clear distinction between the two instances. The  $Q_2$  values of the two graphs (at zero temperature) are plotted as a function of  $s$  in Fig. 1. In this  $N = 16$  case, both graphs have the same ‘classical’ ground-state energy of  $E_G = \langle \hat{H}_p(G) \rangle = -16$  albeit with different degeneracies, namely 21 and 45 (ignoring the fact that each of these states is doubly-degenerate on account of the bit-flip symmetry).

The next family of SRGs that contains more than one member is that with  $N = 25$  vertices. This family has 15 distinct graphs with signature  $(25, 12, 5, 6)$ . Here, finding the ground-state of the Hamiltonian Eq. (1) numerically for the various instances and for different  $s$  values is very resource-demanding and time-consuming yet not impossible. We find that looking at the values of  $Q_2$  and  $M_x$  in the ground state in the limit of  $s \rightarrow 1$  using first-order degenerate perturbation theory suffices to distinguish between all but two of the graphs (the latter two share the same  $Q_2$  and  $M_x$  values in the limit). The results are shown in Fig. 2, a scatterplot of  $Q_2$  vs  $M_x$  for all 15 non-isomorphic graphs for  $s \rightarrow 1$ . In this limit, most instances have the same ground-state energy of  $E_G = -34$  except for two instances having a slightly higher energy

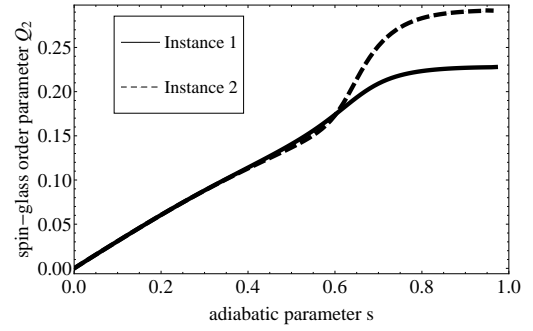


FIG. 1: Spin-glass order parameter  $Q_2$  in the ground state for the two non-isomorphic strongly-regular graphs (SRGs) on  $N = 16$  vertices. As the figure indicates, the two graphs show different  $Q_2$  values starting from  $s \approx 0.4$ .

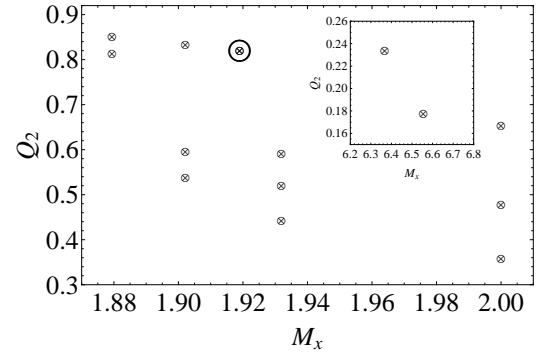


FIG. 2: Scatterplot in the  $M_x - Q_2$  plane of the 15 strongly regular graphs with  $N = 25$  vertices, in the limit  $s \rightarrow 1$ . The horizontal axis corresponds to the magnetization along the  $x$ -direction and the vertical axis stands for the spin-glass order parameter  $Q_2$ . As the figure indicates, our method distinguishes *all graphs* in the family. The circled data point corresponds to the two-graphs undistinguished in the  $s \rightarrow 1$  limit since the values of  $Q_2$  and  $M_x$  are the same. The two instances are nonetheless distinguished by  $s < 1$  measurements (see text). The inset shows the  $M_x - Q_2$  values of two of the graphs that lie outside of the region shown in the main panel are shown.

of  $E_G = -30$ . These correspond to the two points in the inset of Fig. 2. In addition, the circled data point in the figure corresponds to the  $(M_x, Q_2)$  value of the two undistinguished graphs (in the  $s \rightarrow 1$  limit). However, for values of  $s$  less than 1, exact diagonalization reveals a clear distinction between the two graphs. For example, for  $s = 0.73$ , the two graphs have different values of  $Q_2$  in the ground state,  $Q_2 = 0.57914$  and  $0.443423$ .

Perturbation theory-based analysis in the  $s \rightarrow 1$  limit allows us to study families of graphs with  $N = 26, 28$  and  $29$  vertices as well. The degenerate perturbation-theory analysis of the set of 10 SRGs with  $N = 26$  and signature  $(26, 10, 3, 4)$  are shown in Fig. 3 showing a scatterplot in the  $M_x - Q_2$  plane. Here, 7 of the instances were found to have  $E_G = -34$  (with different degeneracies, all of them around  $\sim 1000$ ) and required first-order perturbation theory, whereas the remaining 3 instances had  $E_G = -38$  (with degeneracies 20, 20 and 60), and the leading-order perturbation analysis is of degree 6. Fig. 3 shows that all 10 members of the family are distinguished



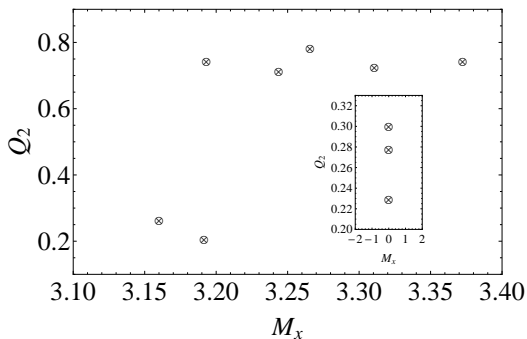


FIG. 3: Scatterplot in the  $M_x - Q_2$  plane of the 10 strongly regular graphs with  $N = 26$  vertices and signature  $(26, 10, 3, 4)$ , in the  $s \rightarrow 1$  limit. As the figure indicates, the annealer distinguishes all graphs in the family.

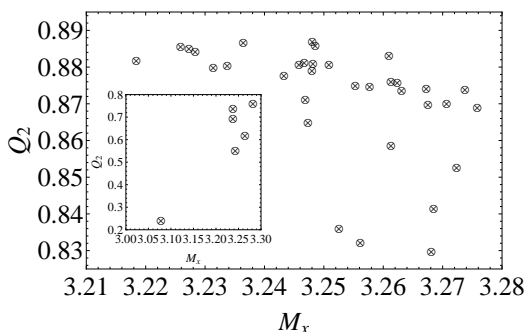


FIG. 4: Scatterplot in the  $M_x - Q_2$  plane of the 41 strongly regular graphs with  $N = 29$  vertices, in the  $s \rightarrow 1$  limit. As the figure indicates, the annealer distinguishes all graphs in the family. The inset shows data points that are out of the range presented in the main panel.

in that plane. The inset shows data points that lie outside of the range presented in the main panel.

For  $N = 28$ , the family  $(28, 12, 6, 4)$  contains 4 distinct graphs. There too, we find that it is sufficient to look at the  $Q_2$  value in the  $s \rightarrow 1$  limit. For three of the four graphs that have the ground-state energy of  $E_G = -28$  (and with different degeneracies, all of them around  $\sim 6000$ ) the  $Q_2$  values are 0.137461, 0.141957 and 0.132883. The fourth graph has a different energy of  $E_G = -24$  (with a degeneracy of 972265).

The largest size of graphs that we deal with analytically using perturbation theory is the family of 41 graphs having  $N = 29$  vertices and signature  $(29, 14, 6, 7)$ . A scatterplot in the  $M_x - Q_2$  plane for this family is given in Fig. 4. While some of the values shown in the scatterplot lie close to one another, all pairs  $(M_x, Q_2)$  are distinct (and can be further differentiated by measurements of other observables) so all non-isomorphic graphs of this family can be distinguished. Here, all members were found to have the same energy of  $E_G = -41$  and with different degeneracies, all of them around  $\sim 3000$ .

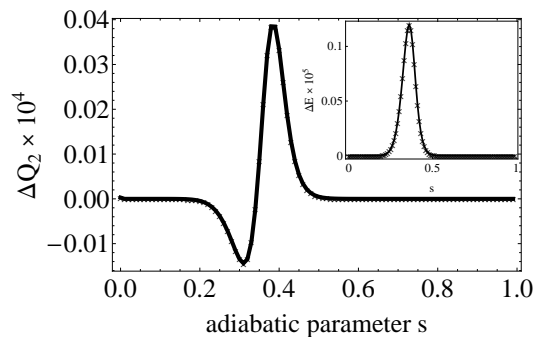


FIG. 5: The difference in  $Q_2$  values,  $\Delta Q_2$  (main panel) and energies (inset), for the two graphs  $G_1$  and  $G_2$  with  $N = 14$  that certain quantum walkers cannot distinguish [37, 38].

## B. Other pairs of graphs

Strongly-regular graphs are of course only one of many classes of graphs that are considered difficult to distinguish. Here, we discuss two regular (rather than strongly-regular) pairs of graphs that are known to be difficult to distinguish (and were, in fact, constructed to be as such). The first pair, which we denote here as  $(G_1, G_2)$  was first considered by Emms *et al.* [37, 38] (the reader is referred Appendix C for the adjacency matrices of the two graphs). The two graphs are regular having 14 vertices. They were given as an example of non isomorphic graphs that can not be distinguished by certain quantum random walkers.

The two graphs, while having almost identical adjacency matrices and therefore also almost identical energies and  $Q_2$  values for  $s \rightarrow 1$ , can still be distinguished by our quantum annealer, at least within a small region of  $s$ . This can be seen by looking at differences in  $Q_2$  values (and smaller but visible differences in the energy). These are shown in Fig. 5. Interestingly, this region precisely corresponds to the quantum phase transition normally seen in quantum adiabatic computing procedures and that is characterized by a small gap [48, 49]. This region is therefore the usual ‘bottleneck’ of the Quantum Adiabatic Algorithm.

We also considered another pair of non-isomorphic regular graphs on 16 vertices, denoted here by  $G_3$  and  $G_4$  (the reader is referred Appendix C for the adjacency matrices of the two graphs), that are known to be difficult to distinguish [50, 51]. Similarly to the previous pair  $(G_1, G_2)$ , the pair  $(G_3, G_4)$  can be distinguished by looking at the  $Q_2$  and energy differences as a function of  $s$ , see Fig. 6.

## V. CONCLUSIONS

In this paper, we have provided a ‘proof of concept’ for a quantum annealer to be a very good candidate for solving the GI problem, i.e., to distinguish between non-isomorphic graphs. The results we presented here sup-

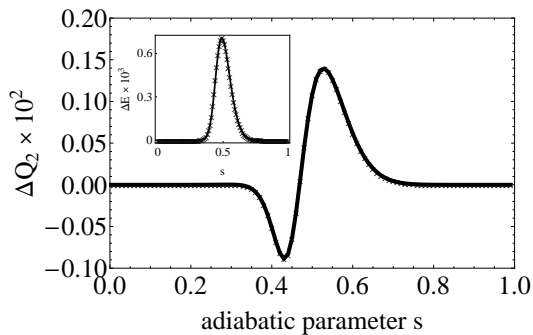


FIG. 6: The difference in  $Q_2$  values,  $\Delta Q_2$  (main panel) and energies (inset), for the two graphs  $G_3$  and  $G_4$  with  $N = 16$  that certain quantum walkers cannot distinguish [51].

port a conjecture that the Quantum Adiabatic prescription can indeed differentiate between all non-isomorphic graphs. Naturally, this conjecture needs to be tested more thoroughly both by exact methods and by numerical simulations of quantum systems and also by conducting experiments on real quantum annealers.

In future studies, other types of graphs or graphs of yet larger sizes need to be tested. It would be interesting to verify that the method works for SRG families of larger sizes than those tested here. Another class of graphs that could generate interesting results is the so called Cai, Fürer and Immerman graph constructions [52], nontrivial examples of which are too large to study with the methods used here.

It is also important to understand the efficiency of the algorithm we propose. To be more precise, how does

the running time of the algorithm scale with graph sizes? This could be tested in various ways and might have important implications on the capabilities of the quantum annealers and adiabatic computation. Another interesting aspect that is of interest as much as it is important is the effect of low yet nonzero temperature on the distinguishing capabilities of the annealer. These however will be the subject of another study.

An attractive feature of the method proposed here is that it can be readily implemented by existing (albeit prototypical) quantum annealers. The method presented here requires a quantum annealer that is capable of Ising-spin interactions of finite connectivity with the addition of constant transverse magnetic fields. The prototypical “D-Wave One” machine [16] is an example that has these capabilities. The results presented here can therefore be experimentally verified and further generalized, and in turn may serve as a powerful example of the potential inherent in quantum annealers.

### Acknowledgments

We thank Kenneth Rudinger and Susan Coppersmith for useful discussions and comments. We acknowledge partial support by the National Security Agency (NSA) under Army Research Office (ARO) contract number W911NF-09-1-0391, and in part by the National Science Foundation under Grant No. DMR-0906366.

- 
- [1] L. M. K. Vandersypen, M. Steffen, G. Breyta, C. S. Yannoni, M. H. Sherwood, and I. L. Chuang, *Nature* **414**, 883887 (2001).
  - [2] Z. Bian, F. Chudak, W. G. Macready, L. Clark, and F. Gaitan (2012), (arXiv:1201.1842).
  - [3] J. Clarke and F. K. Wilhelm, *Nature* **453**, 1031 (2008).
  - [4] A. Friedenauer, H. Schmitz, J. T. Glueckert, D. Porras, and T. Schaetz, *Nature Physics* **4**, 757 (2008).
  - [5] G. K. Brennen, C. M. Caves, P. S. Jessen, and I. H. Deutsch, *Phys. Rev. Lett.* **82**, 10601063 (1999).
  - [6] L. E. Fedichkin, M. V. Yanchenko, and K. A. Valiev, *Quantum Computers and Computing* **1**, 58 (2000).
  - [7] M. A. Nielsen and I. L. Chuang, *Quantum Computation and Quantum Information* (Cambridge University Press, Cambridge, England, 2000).
  - [8] R. Raussendorf and H. J. Briegel, *Phys. Rev. Lett.* **86**, 5188 (2001).
  - [9] R. Raussendorf, D. E. Browne, and H. J. Briegel, *Phys. Rev. A* **68**, 022312 (2003).
  - [10] C. Nayak, S. H. Simon, A. Stern, M. Freedman, and S. Das Sarma, *Rev. Mod. Phys.* **80**, 1083 (2008).
  - [11] G. P. Collins, *Scientific American* **March**, 57 (2006).
  - [12] T. Kadowaki and H. Nishimori, *Phys. Rev. E* **58**, 5355 (1998).
  - [13] E. Farhi, J. Goldstone, S. Gutmann, J. Lapan, A. Lundgren, and D. Preda, *Science* **292**, 472 (2001), The QAA is similar to Quantum Annealing proposed by T. Kadowaki and H. Nishimori, *Phys. Rev. E*, **58**, 5355 (1998).
  - [14] E. Farhi, J. Goldstone, S. Gutmann, J. Lapan, A. Lundgren, and D. Preda, *Science* **292**, 472 (2001), a longer version of the paper appeared in arXiv:quant-ph/0104129.
  - [15] N. Xu, J. Zhu, D. Lu, X. Zhou, X. Peng, and J. Du, <http://arxiv.org/abs/1111.3726v1> (2011).
  - [16] M. W. Johnson, M. H. S. Amin, S. Gildert, T. Lanting, F. Hamze, N. Dickson, R. Harris, A. J. Berkley, J. Johansson, P. Bunyk, et al., *Nature* **473**, 194198 (2011).
  - [17] F. Gaitan and L. Clark, *Phys. Rev. Lett.* **108**, 010501 (2012), (arXiv:1103.1345).
  - [18] D. A. Spielman, in *Proceedings of the twenty-eighth annual ACM symposium on Theory of computing* (1996), STOC '96, pp. 576–584.
  - [19] P. W. Shor, in *Proc. 35th Symp. on Foundations of Computer Science*, edited by S. Goldwasser (1994), p. 124.
  - [20] S. U., *J. Comp. Syst. Sci.* **37**, 312 (1988).
  - [21] T. Rudolph, arXiv:quant-ph/0206068v1 (2002).
  - [22] V. Gudkov and S. Nussinov, arXiv:cond-mat/0209112v2 (2002).
  - [23] S. Shiao and S. Joynt, R. Coppersmith, *Quantum Inf. Comput.* **5**, 492 (2005).
  - [24] J. K. Gamble, M. Friesen, D. Zhou, R. Joynt, and S. N. Coppersmith, *Phys. Rev. B* **81**, 052313 (2010).
  - [25] K. Rudinger, J. K. Gamble, M. Wellons, E. Bach,

- M. Friesen, R. Joynt, and S. N. Coppersmith (2012), arXiv:1206.2999.
- [26] A. Y., D. L., and Z. N., Phys. Rev. A **48**, 1687 (1993).
- [27] E. Bach, S. Coppersmith, M. P. Goldschen, R. Joynt, and J. Watrous, J. Comp. Syst. Sci. **69**, 562 (2004).
- [28] Solenov, D., and F. L., Phys. Rev. A **73**, 012313 (2006).
- [29] A. Childs, E. Farhi, and S. Gutmann, Quantum Inf. Process. **1**, 35 (2002).
- [30] N. Shenvi, J. Kempe, and K. B. Whaley, Phys. Rev. A **67**, 052307 (2003).
- [31] A. Ambainis, International Journal of Quantum Information **1**, 507 (2003).
- [32] A. Ambainis, in *Annual IEEE Symposium on Foundations of Computer Science* (2004), vol. 0, p. 22.
- [33] F. Magniez, A. Nayak, J. Roland, and M. Santha, in *Proceedings of the thirty-ninth annual ACM symposium on Theory of computing (ACM, New York, NY, USA, 2007)* (2007), STOC '07, p. 575.
- [34] V. Potoček, A. Gábris, T. Kiss, and I. Jex, Phys. Rev. A **79**, 012325 (2009).
- [35] D. Reitzner, M. Hillery, E. Feldman, and V. Bužek, Journal of Physics A Mathematical General **79**, 012323 (2009).
- [36] B. Douglas and J. Wang, J. Phys. A: Mathematical and Theoretical **41**, 075303 (2008).
- [37] D. Emms, E. Hancock, S. Severini, and R. Wilson, Electr. J. Comb. **13** (2006).
- [38] D. Emms, S. Severini, R. Wilson, and E. Hancock, Pattern Recognition **42**, 1988 (2009).
- [39] T. Kato, J. Phys. Soc. Jap. **5**, 435 (1951).
- [40] A. Messiah, *Quantum Mechanics* (North-Holland, Amsterdam, 1962).
- [41] M. Mézard and G. Parisi, Eur. Phys. J. B **20**, 217 (2001).
- [42] M. Mézard and G. Parisi, Journal of Statistical Physics **111**, 1 (2003), (arXiv:cond-mat/0207121).
- [43] L. Zdeborová and S. Boettcher, Journal of Statistical Mechanics: Theory and Experiment **2**, 20 (2010), 0912.4861.
- [44] E. Farhi, D. Gosset, I. Hen, A. W. Sandvik, P. Shor, A. P. Young, and F. Zamponi (2012), (unpublished).
- [45] E. W. Weisstein, *Strongly regular graph*, from MathWorld—A Wolfram Web Resource., URL <http://mathworld.wolfram.com/StronglyRegularGraph.html>.
- [46] E. Spence, *Strongly regular graphs on at most 64 vertices*, URL <http://www.maths.gla.ac.uk/~es/srgraphs.html>.
- [47] B. McKay, *Combinatorial data*, URL <http://cs.anu.edu.au/~bdm/data/graphs.html>.
- [48] A. P. Young, S. Knysh, and V. N. Smelyanskiy, Phys. Rev. Lett. **101**, 170503 (2008), (arXiv:0803.3971).
- [49] A. P. Young, S. Knysh, and V. N. Smelyanskiy, Phys. Rev. Lett. **104**, 020502 (2010), (arXiv:0910.1378).
- [50] C. Godsil and G. Royle, *Algebraic Graph Theory* (Springer, New York, 2001).
- [51] K. J. Guo, Ph.D. thesis, University of Waterloo (2010).
- [52] J. Y. Cai, M. Fürer, and N. Immerman, in *Proceedings of the 30th Annual Symposium on Foundations of Computer Science (Washington, DC, USA) (1989)*, SFCS '89, pp. 612–617, IEEE Computer Society.

## Appendix A: Conjugate gradient method

In what follows we explain in some detail the specific conjugate-gradient method that was used in this study

to calculate the ground state and corresponding energy of a given Hamiltonian. We found that usual Lanczos and conjugate-gradient methods are not sufficiently accurate in some cases for certain measurable quantities, and therefore somewhat novel variants of these are needed to obtain accurate calculations, as will be explained below.

Here, we shall discuss the use of the conjugate-gradient method to find the ground state and the corresponding energy of a given Hamiltonian  $\hat{H}$ . Within this method, the minimization of the energy is obtained by minimizing:

$$E_0 = \min f(|\psi\rangle) = \min_{\{|\psi\rangle\}} \frac{\langle\psi|\hat{H}|\psi\rangle}{\langle\psi|\psi\rangle} \quad (\text{A1})$$

The key feature here is that the objective function  $f$  has no local minima but only one global minimum that is to be found. In principle any minimization method would work. The question is how well. After choosing a basis  $\{|n\rangle\}$  to work in, one can write  $|\psi\rangle = \sum c_n |n\rangle$  and the objective function to be minimized becomes:

$$\begin{aligned} E_0 &= \min f(\{c_n\}) \\ &= \min_{\{c_n\}} \frac{\sum_n c_n^2 d_n + \sum_n c_n \sum_m a_{nm} c_m}{\sum_n |c_n|^2}. \end{aligned} \quad (\text{A2})$$

In the above equation we denoted the diagonal elements of the Hamiltonian by  $\hat{H}_{ii} = d_i$  and the off-diagonal elements (which are presumably sparse) by  $\hat{H}_{ij} = a_{ij}$ . In what follows we shall assume that the coefficients  $c_n$  are real-valued for convenience. The generalization to complex-valued coefficients is trivial.

Employing the conjugate gradient method in this case is very simple. Firstly, the gradient with respect to the various parameters  $c_n$  is easily obtainable:

$$\begin{aligned} \frac{\partial f}{\partial c_k} &= \frac{2d_k c_k + 2 \sum_m a_{km} c_m}{\sum_n |c_n|^2} \\ &- \frac{2c_k (\sum_n |c_n|^2 d_n + \sum_n c_n \sum_m a_{nm} c_m)}{(\sum_n |c_n|^2)^2} \end{aligned} \quad (\text{A3})$$

Secondly, the one-dimensional minimization steps of the conjugate gradient method can be calculated explicitly

$$\begin{aligned} \min_{\alpha} f(|\psi\rangle + \alpha|\delta\rangle) &= \\ \min_{\alpha} \frac{\langle\delta|\hat{H}|\delta\rangle\alpha^2 + 2\text{Re}\langle\psi|\hat{H}|\delta\rangle\alpha + \langle\psi|\hat{H}|\psi\rangle}{\langle\delta|\delta\rangle\alpha^2 + 2\text{Re}\langle\psi|\delta\rangle\alpha + \langle\psi|\psi\rangle}. \end{aligned} \quad (\text{A4})$$

The above expression is minimized for some easily obtainable  $\alpha^*$  that is one of the two solutions of a quadratic equation, and that produces the minimum (along the line) energy of:

$$\begin{aligned} E_0 &= f(|\psi\rangle + \alpha^*|\delta\rangle) \\ &= \frac{\langle\delta|\hat{H}|\delta\rangle\alpha^{*2} + 2\text{Re}\langle\psi|\hat{H}|\delta\rangle\alpha^* + \langle\psi|\hat{H}|\psi\rangle}{\langle\delta|\delta\rangle\alpha^{*2} + 2\text{Re}\langle\psi|\delta\rangle\alpha^* + \langle\psi|\psi\rangle} \end{aligned} \quad (\text{A5})$$

## 1. Variable offset minimization

Inaccuracies in the minimization of the energy may often result from the addition of terms with different orders of magnitude. This follows from the floating-point nature of these calculations (be it single- or double-precision). While this may not affect the value of the energy reached by the minimization as much, the impact on the ground-state coefficients and therefore also the expectation values of different observables may be decisive. For example, if the diagonal energy term  $\sum_n c_n^2 d_n$  differs in orders of magnitude from the off-diagonal energy term  $\sum_n c_n \sum_m a_{nm} c_m$ , then this could lead to severe inaccuracies in the various measurable quantities. How can one make sure that the diagonal energy and the off-diagonal energies have the same order of magnitude.

A simple way that we have found to work very well in practice is to offset the diagonal term in each step such that the total energy is kept equal to zero, meaning that the diagonal and off-diagonal terms are equal in magnitude (and opposite in sign). This is simply done by shifting the diagonal elements  $d_n \rightarrow d_n + \epsilon$ , choosing the constant  $\epsilon$  in each step in such a way that the total energy (diagonal plus non-diagonal) is zero. From the equality:

$$\begin{aligned} & \frac{\sum_n c_n^2 (d_n + \epsilon) + \sum_n c_n \sum_m a_{nm} c_m}{\sum_n |c_n|^2} \quad (\text{A6}) \\ &= \frac{\sum_n c_n^2 d_n + \sum_n c_n \sum_m a_{nm} c_m}{\sum_n |c_n|^2} + \epsilon, \end{aligned}$$

it follows that offsetting the objective function by  $\epsilon$  will not change the amplitudes  $c_n$ , and so will also not affect the gradients. Its only effect is to offset the minimum energy to zero at each step. The fact that the value to be reached within the minimization is zero increases the accuracy of the computation. The resulting ground-state energy at the end of the process will be in fact stored in the variable offset  $E_0 = \epsilon$ .

## 2. Minimizing the residuals

Once the energy  $E_0$  is measured to great precision, we followed this up with a second stage of minimizing the residuals, i.e., perform the conjugate gradient routine on the objective function:

$$f = \min_{\{|\psi\rangle\}} \frac{\langle \psi | \hat{H}^2 | \psi \rangle - 2E_0 \langle \psi | \hat{H} | \psi \rangle + E_0^2 \langle \psi | \psi \rangle}{\langle \psi | \psi \rangle}. \quad (\text{A7})$$

## Appendix B: Properties of Graphs and Strongly Regular Graphs (SRGs)

A graph  $G = (V, E)$  is a set of vertices  $V$  and edges  $E$ . The vertices are usually labeled by inte-

ger indices, and the edges are unordered pairs of vertices. Two vertices that form an edge are said to be *connected* and are described as *neighbors*. Two vertices that are not connected by an edge are *disconnected*. The total number of neighboring vertices of a particular vertex is called its *degree*. For example, the graph  $G = (\{1, 2, 3, 4\}, \{(1, 2), (2, 3), (3, 4), (4, 1)\})$  is a cycle graph with four vertices. Two graphs are *isomorphic* if they can be made identical by relabeling their vertices. For example, the graph  $H = (\{1, 2, 3, 4\}, \{(1, 3), (3, 2), (2, 4), (4, 1)\})$  is isomorphic to  $G$ , since after relabeling  $2 \leftrightarrow 3$ , the two graphs are equivalent.

Graphs are conveniently expressed algebraically as *adjacency matrices*. An adjacency matrix  $A$  of a graph with  $N$  vertices is an  $N \times N$  matrix in the basis of vertex labels, with  $A_{ij} = 1$  if vertices  $i$  and  $j$  are connected by an edge, and zero otherwise. The adjacency matrix for the graph  $G$  is

$$\mathbf{A}_G = \begin{pmatrix} 0 & 1 & 0 & 1 \\ 1 & 0 & 1 & 0 \\ 0 & 1 & 0 & 1 \\ 1 & 0 & 1 & 0 \end{pmatrix}. \quad (\text{B1})$$

The *spectrum* of a graph is the eigenvalue spectrum of its adjacency matrix. The spectrum of  $G$  is  $\{-2, 0, 2\}$ , with 0 two-fold degenerate.

The adjacency matrix of any strongly regular graph (SRG) satisfies the useful relation [50]:

$$\mathbf{A}^2 = (k - \mu)\mathbf{I} + \mu\mathbf{J} + (\lambda - \mu)\mathbf{A}, \quad (\text{B2})$$

where  $\mathbf{I}$  is the identity,  $\mathbf{J}$  is the matrix of all ones ( $J_{ij} = 1$  for all  $i, j$ ), and the parameters  $k, \mu$  and  $\lambda$  label properties of a family of SRG's, as discussed in Sec. IV A of the text. Since  $\mathbf{J}^2 = N\mathbf{J}$  and  $\mathbf{I}^2 = \mathbf{I}$ , this forms a three-dimensional algebra, and we can write

$$\mathbf{A}^n = \alpha_n \mathbf{I} + \beta_n \mathbf{J} + \gamma_n \mathbf{A}, \quad (\text{B3})$$

where the coefficients  $\alpha_n, \beta_n$ , and  $\gamma_n$  are functions only of the family parameters,  $k, \mu$  and  $\lambda$ .

Using the stringent constraints placed on SRGs, one can show that, regardless of size, the spectrum of any SRG has only three distinct values [50]:

$$\lambda_0 = -k, \quad (\text{B4})$$

which is non-degenerate, and

$$\lambda_{1,2} = -\frac{1}{2} \left( \lambda - \mu \pm \sqrt{N} \right), \quad (\text{B5})$$

which are both highly degenerate. Both the value and degeneracy of these eigenvalues depend only on the family parameters, so within a particular SRG family, all graphs are cospectral [50]. These highly degenerate spectra are one reason why distinguishing non-isomorphic SRGs is difficult.



### Appendix C: Non-SRG graphs

Here we provide the adjacency matrices studied in Sec. IV B. Both  $G_1$  and  $G_2$  are regular graphs on 14 vertices with valency 4 and are found in [37, 38]. The graph  $G_1$  is given by the adjacency matrix:

$$\mathbf{A}_{G_1} = \begin{pmatrix} 0 & 1 & 0 & 0 & 0 & 0 & 0 & 1 & 0 & 0 & 0 & 0 & 1 & 1 \\ 1 & 0 & 0 & 0 & 0 & 0 & 0 & 0 & 1 & 1 & 0 & 0 & 1 & 0 \\ 0 & 0 & 0 & 1 & 0 & 0 & 0 & 0 & 1 & 1 & 0 & 0 & 0 & 1 \\ 0 & 0 & 1 & 0 & 0 & 1 & 0 & 1 & 1 & 0 & 0 & 0 & 0 & 0 \\ 0 & 0 & 0 & 0 & 0 & 1 & 0 & 0 & 0 & 1 & 1 & 0 & 0 & 1 \\ 0 & 0 & 0 & 1 & 1 & 0 & 1 & 0 & 0 & 0 & 1 & 0 & 0 & 0 \\ 0 & 0 & 0 & 0 & 0 & 1 & 0 & 1 & 0 & 0 & 0 & 1 & 0 & 1 \\ 1 & 0 & 0 & 1 & 0 & 0 & 1 & 0 & 0 & 0 & 0 & 1 & 0 & 0 \\ 0 & 1 & 1 & 1 & 0 & 0 & 0 & 0 & 0 & 0 & 0 & 1 & 0 & 0 \\ 0 & 1 & 1 & 0 & 1 & 0 & 0 & 0 & 0 & 0 & 1 & 0 & 0 & 0 \\ 0 & 0 & 0 & 0 & 1 & 1 & 0 & 0 & 0 & 1 & 0 & 0 & 1 & 0 \\ 0 & 0 & 0 & 0 & 0 & 1 & 1 & 1 & 0 & 0 & 0 & 1 & 0 & 0 \\ 1 & 1 & 0 & 0 & 0 & 0 & 0 & 0 & 0 & 0 & 1 & 1 & 0 & 0 \\ 1 & 0 & 1 & 0 & 1 & 0 & 1 & 0 & 0 & 0 & 0 & 0 & 0 & 0 \end{pmatrix}, \quad (\text{C1})$$

and the graph  $G_2$  is obtained by  $G_1$  by replacing the entries (1, 2) and (3, 4) with entries (1, 3) and (2, 4) (and corresponding transposed entries). It can be verified that  $G_1$  is not isomorphic to  $G_2$ .

Graphs  $G_3$  and  $G_4$ , also studied in Sec. IV B, are regular graphs on 16 vertices with valency 3 and can be found in Ref. [51]. The graph  $G_3$  is given by the adjacency matrix:

$$\mathbf{A}_{G_3} = \begin{pmatrix} 0 & 0 & 1 & 1 & 0 & 0 & 0 & 0 & 0 & 0 & 0 & 1 & 0 & 0 & 0 & 0 \\ 0 & 0 & 0 & 0 & 1 & 1 & 0 & 0 & 0 & 0 & 0 & 0 & 1 & 0 & 0 & 0 \\ 1 & 0 & 0 & 0 & 1 & 0 & 0 & 0 & 0 & 0 & 0 & 0 & 0 & 1 & 0 & 0 \\ 1 & 0 & 0 & 0 & 0 & 1 & 0 & 0 & 0 & 0 & 0 & 0 & 0 & 0 & 1 & 0 \\ 0 & 1 & 1 & 0 & 0 & 1 & 0 & 0 & 0 & 0 & 0 & 0 & 0 & 0 & 0 & 0 \\ 0 & 1 & 0 & 1 & 1 & 0 & 0 & 0 & 0 & 0 & 0 & 0 & 0 & 0 & 0 & 0 \\ 0 & 0 & 0 & 0 & 0 & 0 & 0 & 1 & 1 & 1 & 0 & 0 & 0 & 0 & 0 & 0 \\ 0 & 0 & 0 & 0 & 0 & 0 & 1 & 0 & 1 & 0 & 1 & 0 & 0 & 0 & 0 & 0 \\ 0 & 0 & 0 & 0 & 0 & 0 & 1 & 1 & 0 & 0 & 0 & 1 & 0 & 0 & 0 & 0 \\ 0 & 0 & 0 & 0 & 0 & 0 & 1 & 0 & 0 & 0 & 0 & 0 & 1 & 1 & 0 & 0 \\ 0 & 0 & 0 & 0 & 0 & 0 & 1 & 0 & 0 & 0 & 0 & 0 & 1 & 0 & 1 & 0 \\ 1 & 0 & 0 & 0 & 0 & 0 & 0 & 1 & 0 & 0 & 0 & 0 & 0 & 0 & 0 & 1 \\ 0 & 1 & 0 & 0 & 0 & 0 & 0 & 0 & 0 & 1 & 1 & 0 & 0 & 0 & 0 & 0 \\ 0 & 0 & 1 & 0 & 0 & 0 & 0 & 0 & 1 & 0 & 0 & 0 & 0 & 0 & 0 & 1 \\ 0 & 0 & 0 & 1 & 0 & 0 & 0 & 0 & 0 & 1 & 0 & 0 & 0 & 0 & 0 & 1 \\ 0 & 0 & 0 & 0 & 0 & 0 & 0 & 0 & 0 & 0 & 1 & 0 & 1 & 1 & 0 & 0 \end{pmatrix}, \quad (\text{C2})$$

and the adjacency matrix of  $G_4$  is obtained from that of  $G_3$  by inverting the entries (i.e. interchanging ones with zeros) belonging to the sub-matrix spanned by rows (1, 2) and columns (3, 4, 5, 6) along with the corresponding transposed entries.